PAPER

Multi-cycling nanoindentation in additively manufactured Inconel 625 before and after laser peening

To cite this article: Ali Tajyar *et al* 2022 *Surf. Topogr.: Metrol. Prop.* **10** 025031

IOP Publishing Surf. Topogr.: Metrol. Prop. **10** (2022) 025031 https://doi.org/10.1088/2051-672X/ac7736

Surface Topography: Metrology and Properties

RECEIVED
6 March 2022

REVISED
20 April 2022

ACCEPTED FOR PUBLICATION
9 June 2022

PUBLISHED
22 June 2022

PAPER

Multi-cycling nanoindentation in additively manufactured Inconel 625 before and after laser peening

Ali Tajyar[1], Nicholas Brooks[1], Majid Vaseghi[1], Lloyd Hackel[2], Kasra Momeni[1] and Keivan Davami[1,*]

[1] Department of Mechanical Engineering, The University of Alabama, Tuscaloosa, AL, United States of America
[2] Metal Improvement Company, Surface Technologies, Curtiss Wright, Livermore, CA, United States of America
[*] Author to whom any correspondence should be addressed.

E-mail: kdavami@eng.ua.edu

Keywords: multi-cycle nanoindentation, inconel 625, laser peening, surface fatigue, mechanical characterization

Abstract

In this research, a room temperature multicycle nanoindentation technique was implemented to evaluate the effects of the laser peening (LP) process on the surface mechanical behavior of additively manufactured (AM) Inconel 625. Repetitive deformation was introduced by loading-unloading during an instrumented nanoindentation test on the as-built (No LP), 1-layer, and 4-layer laser peened (1LP and 4LP) conditions. It was observed that laser-peened specimens had a significantly higher resistance to penetration of the indenter and lower permanent deformation. This is attributed to the pre-existing dislocation density induced by LP in the material which affects the dislocation interactions during the cyclic indentation. Moreover, high levels of compressive stresses, which are greater in the 4LP specimen than the 1LP specimen, lead to more effective improvement of surface fatigue properties. The transition of the material response from elastic-plastic to almost purely elastic in 4LP specimens was initiated much earlier than it did in the No LP, and 1LP specimens. In addition to the surface fatigue properties, hardness and elastic modulus were also evaluated and compared.

1. Introduction

Inconel 625 (IN 625) is a solid-solution, nickel-chromium-niobium-molybdenum alloy with outstanding resistance to high temperature and corrosive environments as well as excellent creep and fatigue characteristics [1, 2]. This material has drawn particular interest in various industrial sectors including power generation, aeronautical, marine, and petrochemical applications, due to its excellent attributes [3–5]. In recent years an additive manufacturing technology coined laser powder bed fusion (LPBF) has emerged as a successful tool for the fabrication of IN 625 parts with high density, good surface finish, and mechanical properties [6–9]. This technique has received significant attention, particularly for the fabrication of complex structures. However, defects and residual tensile stresses from the manufacturing process have been a source of concern. A combination of AM techniques with additional post-processing surface treatment techniques can offer a solution to these challenges.

Surface engineering techniques such as LP, shot peening, and ultrasonic peening are broadly used to enhance the material and mechanical properties of components including fatigue, fretting fatigue, wear, and stress corrosion cracking [10–13]. LP is an emerging surface treatment technique which allows for precise control over process parameters and provides enhanced resistance to crack initiation and improved fatigue resistance. Instead of the thermal effects of the laser, LP employs intense laser pulses with pulse energies up to 50 J and duration of 8 to 50 ns to create shocks at the surface of the material. These pressure shocks propagate into the material and plastically strain it. The deformation by shock plastically compresses the material perpendicular to the surface. Due to the Poisson effect, the metal expands transversely to conserve volume. Surrounding material counters the expansion, generating a residual compressive stress field near the surface and relatively deep into the subsurface regions. High strain rate plastic deformation generates a high density of dislocations as well. The compressive stress field, as well as the modified microstructure, act like a shield in the plastically deformed

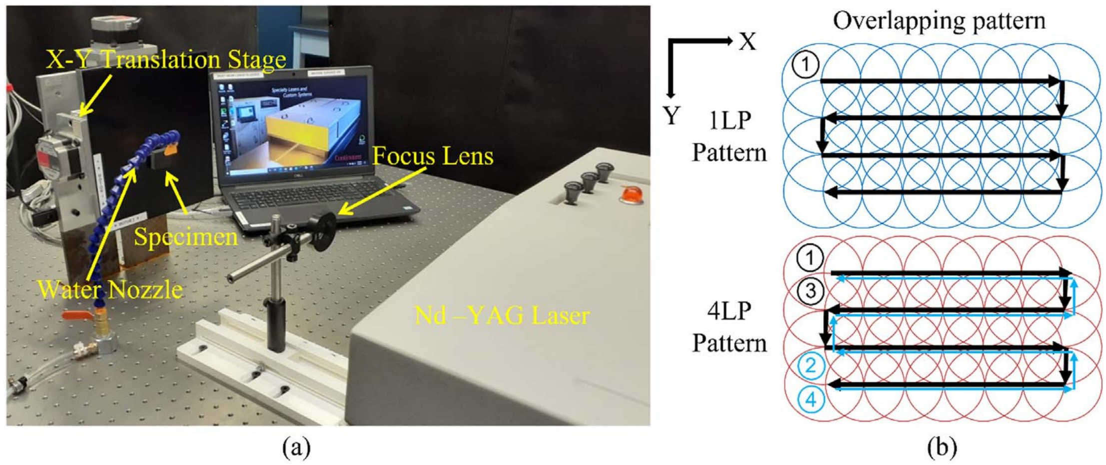

Figure 1. (a) Experimental setup and (b) the laser paths illustrating the overlapping pattern used during LP of specimens 1LP and 4LP.

Table 1. Chemical composition of powderized alloy.

Element	Ni	Cr	Fe	Nb+Ta	Mo	Ti	Al	Co	Mn	Si	Cu
Wt%	50–55	17–21	Balance	4.76–5.5	2.80–3.30	0.65–1.15	0.2–0.8	$\leqslant 1$	$\leqslant 0.35$	$\leqslant 0.35$	$\leqslant 0.30$

Less than 0.1 Wt% of C, S, P, B, Ca, Mg, O, N

layer where a crack will need much more energy to initiate and propagate, and consequently, enhance the material strength against failures initiating there [14–18].

The surface damage caused by the cyclic contact often leads to catastrophic failures of mechanical parts. Multicycle indentation techniques can be used to study the surface fatigue performance of the materials [19, 20], surface crack formation [21], and to evaluate the impact of surface treatment techniques on the mitigation of various surface damages. Richter *et al* [22] investigated the mechanical properties of a single phase cubic boron carbide using the multi-cycling nanoindentation technique. The elastic-plastic response of the material was examined using repeated loading-unloading processes. It was reported that the hysteresis loops observed in the material were caused by the initiation of nano-cracks. The cyclic nanoindentation tests were used by Chatterjee *et al* to investigate the effects that grain boundaries play in controlling plastic deformation during cyclic loading [23]. The equal channel angular extrusion process (ECAE) and its influence on the fatigue behavior of Al were evaluated by Peng *et al* using the multicycle indentation technique [24]. It was revealed that the level of dislocation density in the ECAE deformed Al plays an important role in the fatigue performance of the material [24].

The objective of this research is to study the surface fatigue behavior of as-built and LPed IN 625 test specimens where they were subjected to cyclic nanoscale indentation loading. The results depicted in this study clearly indicate the potential of enhancing the durability of IN 625 against surface-initiated failure mechanisms through the implementation of LP.

2. Experiments

2.1. Material

The tests were conducted on AM IN 625 specimens manufactured by the Renishaw AM 250 machine. The specimen dimensions were 33 mm × 26 mm × 8.75 mm. The powder's elemental composition of AM IN 625 is presented in table 1.

2.2. LP process

Surface treatment was carried out using a Q-Switched Nd:YAG laser (Powerlite DLS Plus), operating at a frequency of 10 Hz, a wavelength of 1064 nm, a power density of 6 GW cm^{-2}, and a pulse duration of 8 ns. Single-layer and four-layer of LP treatments were applied to the surface of the specimens. Figure 1(a) shows the experimental setup. A layer of black insulation tape, with a thickness of $\approx$ 250 μm, was placed on the material surface while a flowing water overlay, which acts as the dielectric medium, flowed over the specimen during LP. The main benefits of the transparent overlay are to confine, concentrate, and direct the plasma to the surface of the material [25]. LP was conducted with a 3.0 mm circular spot size and a 50% overlap between spots. For the 4LP treatment, the subsequent layers were offset from the preceding layers by 50% of the spot size (figure 1(b)).

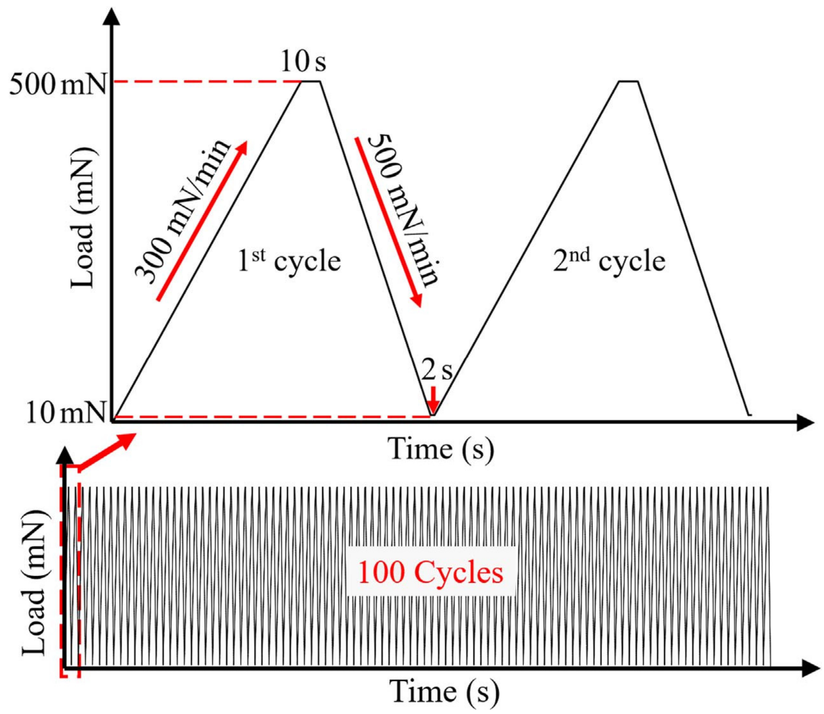

Figure 2. Multicycle nanoindentation protocol.

2.3. Multicycle nanoindentation test

Specimens for the nanoscale characterization were prepared by applying grinding and polishing. Cyclic nanoindentation was performed using a diamond Berkovich indenter in the constant load repetition mode in a nanomechanical test instrument (Anton-Paar, TTX-NHT^2). Following the loading stage, which applied the maximum force to the specimen, the force was decreased to a minimum load. This loading-unloading process continued throughout the testing. Figure 2 shows the multicycle load-time graph, and the indentation parameters are shown in table 2. A constant indentation load of 500 mN was selected to induce an indentation depth up to at least 2500 nm in the specimens. This depth is sufficient enough to ensure that several grains will be involved in the indentation process and ensures that the observed behavior will be reflective of a collection of grains rather than just a few. The number of cycles performed on each specimen was 100 cycles. This was selected to ensure that damage to the tip, which can occur if too many consecutive high-load cycles are performed, would not be significant enough to impact the results. The standard procedure put forth by Oliver and Pharr for determining the hardness and elastic modulus using nanoindentation was utilized for each cycle.

Table 2. Indentation parameters used in multicycle nanoindentation.

Poisson's ratio of IN 625	0.29
Constant loading rate	300 mN min^{-1}
Constant unloading rate	500 mN min^{-1}
Maximum load	500 mN
Minimum load	10 mN
Dwell time at maximum load	10 s
Dwell time between cycles	2 s
Number of cycles	100 times

2.4. Residual stress measurement

Residual stress measurements were conducted using an x-Ray Diffraction based stress analysis system (XRD, Proto iXRD) using a Mn-Kα x-ray source ($\lambda = 2.10314$ Å) and a conventional $\sin^2\psi$ technique was adopted to obtain the surface residual stress values. Prior to each measurement, an alignment and calibration procedure were performed on the device using a stress-free 316 L steel powder sample. The values obtained during calibration were within the acceptable range which was recommended by the manufacturer ($\pm$ 12 MPa). Measurements were performed on the surface of each specimen (No LP, 1LP, and 4LP) 3 times.

2.5. Microstructure characterization

The three specimens (No LP, 1LP, and 4LP) were mounted in conductive resin, ground from 240 to 4000 grit, and then polished using diamond suspensions of 3 and 1 μm. This was followed by a 0.05 μm colloidal silica suspension which was employed to achieve the mirror-like surface finish necessary for investigating the residual impressions post-nanoindentation using scanning electron microscopy (SEM, Thermo Scientific™ Apreo).

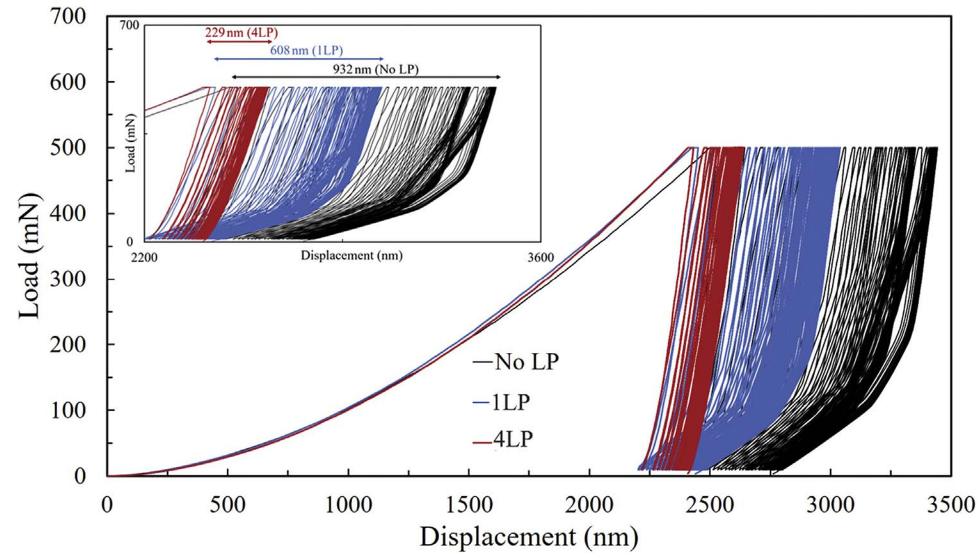

Figure 3. Multicycle load-displacement curves. The inset shows a magnified version of the graph with additional details.

3. Results and discussion

Figure 3 shows the multicycle load-displacement curves obtained for both the No LP and LPed specimens. During the initial loading stage, both elastic and plastic deformation occur in the material. As can be seen in figure 3, No LP and 4LP specimens had the deepest and the least residual indentation depth, respectively, for the same number of cycles of 100 and at a constant force of 500 mN. For an indentation depth of less than 1750 nm in the loading phase, the relationship between the load-displacement curves for the LPed specimens and the No LP specimen coincide well. However, at a depth greater than approximately 1750 nm, a greater force is necessary to reach the same indentation depth for the LPed specimens. This indicates that work hardening for the LPed specimens is greater than that exhibited by the No LP specimen [26, 27]. Although the main portion of plastic deformation occurs during the first cycle, material deformation propagates a bit further following each subsequent cycle. The total penetration depths observed between cycles 2–100 for the No LP, 1LP, and 4LP specimens were 932 nm, 608 nm, and 229 nm, respectively. Also, the permanent deformation that occurred in between cycles 2–100 in each specimen (No LP, 1LP, and 4LP) was 455 nm, 237 nm, and 190 nm, respectively.

Surface treatments such as laser peening induce some dislocations at the surface and sub-surface of the treated material. During indentation of a surface-treated material, the plastic deformation induced by the indenter in the loading portion can be considered as occurring in two stages. During the first stage, geometrically necessary dislocation (GND) nucleation occurs beneath the indenter tip while the radii of the dislocation loops enlarge with increasing indenter depth. In the second stage, pre-existing dislocations, which are

Table 3. Surface residual stress measurements and maximum penetration depth of indenter for specimens (No LP, 1LP, and 4LP).

Specimen	Surface residual stress (MPa)	Maximum penetration depth (nm)
No LP	−203 MPa	3420 nm
1 LP	−540 MPa	3000 nm
4 LP	−616 MPa	2600 nm

induced by surface treatment, can begin to resist the movement of new dislocation loops that are induced during the indentation. The interaction between the new and pre-existing dislocations requires sufficiently large shear stress to influence the growth and gliding of dislocation loops [24]. During unloading, these dislocations rearrange themselves to reduce the internal stresses. This is then followed by the next loading where renewed localized stresses by the tip can induce more dislocations, further expanding the plastic zone [23, 24].

The magnitude of pre-existing dislocation density induced by LP in the material can play an important role in the interaction between dislocations during the cyclic indentation. Johnson's spherical cavity model [28, 29] states that the size of the plastic zone, c, under the indenter can be approximated as follows in equation (1):

$$c = \left(\frac{3F}{2\pi\sigma}\right)^{1/2} \propto F^{1/2}\rho^{-1/4} \qquad (1)$$

where ρ is dislocation density, F is indentation load, and σ is the tensile flow stress. The plastic deformation zone (c) decreases with increasing dislocation density (ρ). LP produces severe plastic deformation on and just beneath the surface of the material and significantly increases the dislocation density in the plastically deformed layer with varying configurations, i.e. dislocation cells and tangles. Thus, by increasing the

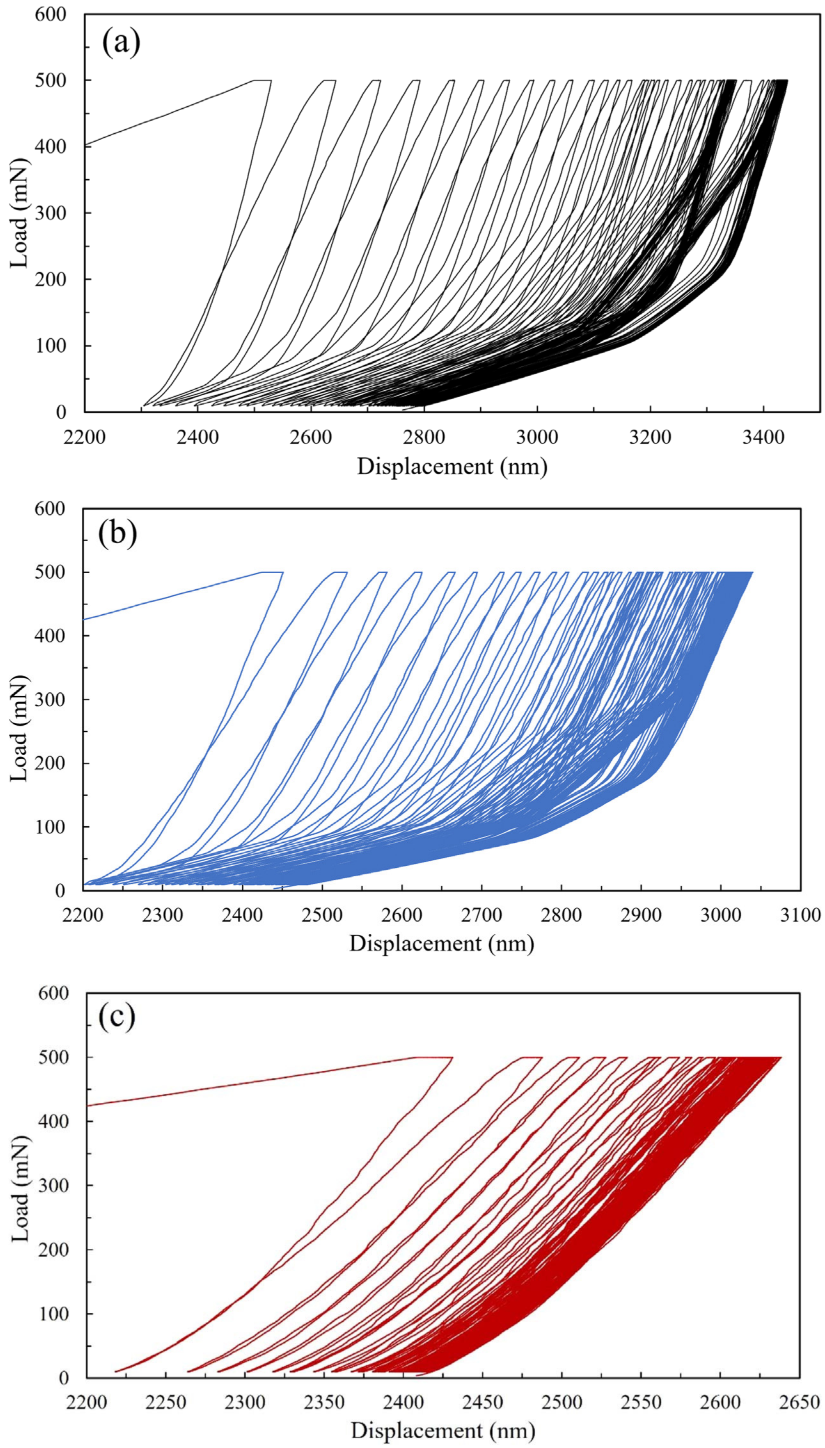

Figure 4. Reload-unload Curves for (a) No LP, (b) 1LP, and (c) 4LP.

number of layers used in LP, the density of the generated dislocations increases [30]. According to equation (1), when there is a higher density of dislocations (ρ), the plastic zone (c) will be smaller. Therefore, it is expected that the plastic zone under the nanoindenter tip will be the smallest for 4LP specimen, and the largest for the specimen without any peening (No LP). This correlates well with what is observed in the recorded displacement in figure 3, where the higher pre-existing dislocation density in the 4LP specimen, compared to that in the No LP specimen, leads to a smaller displacement since the tip has a higher probability of encountering defects. This induces a strong interaction between pre-existing dislocations and the indenter tip and produces a higher resistance to penetration of the indenter in addition to permanent deformation during cyclic indentation.

Additionally, the surface residual stresses for all three specimens were measured using an XRD technique. The XRD measurements and the maximum penetration depth that was realized for each specimen

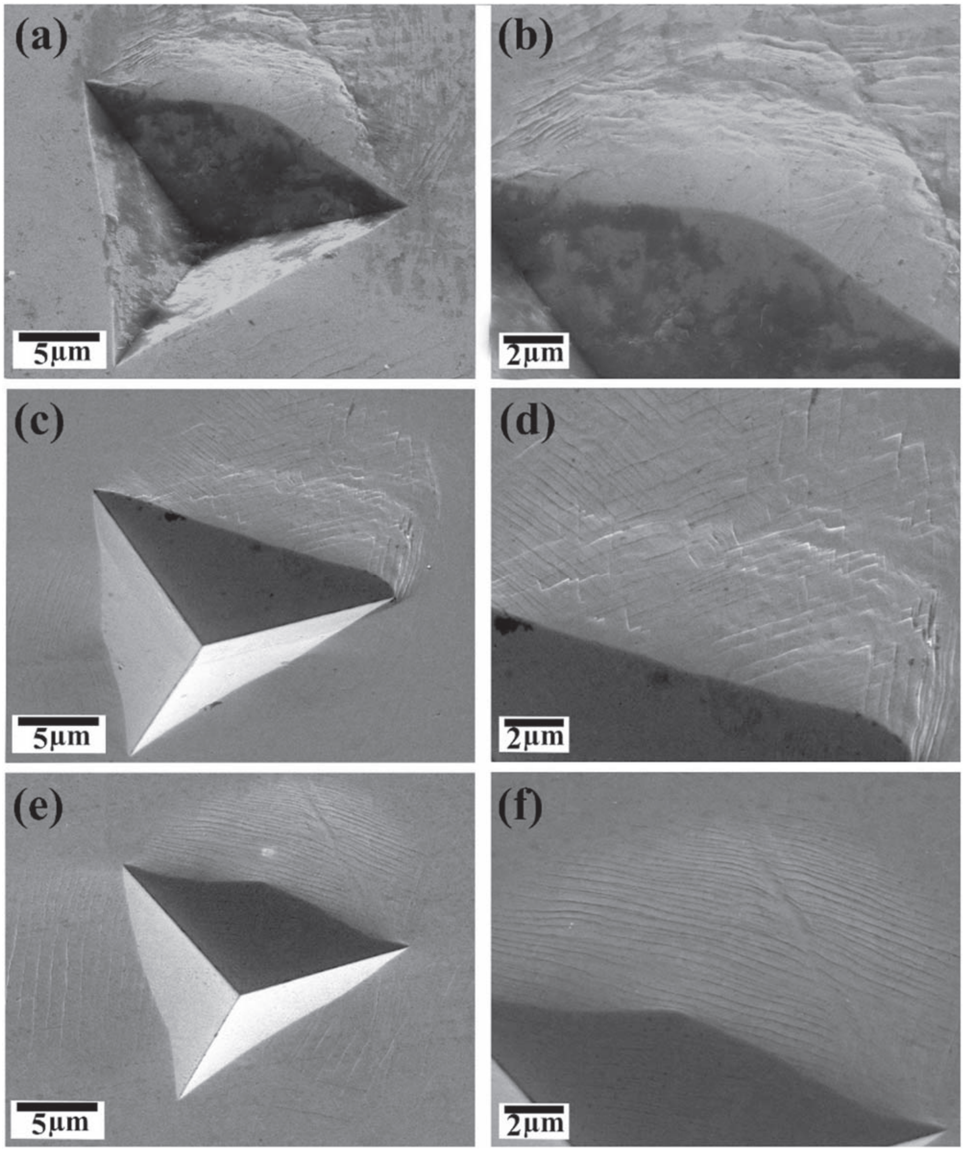

Figure 5. SEM micrographs of residual impressions on (a), (b) No LP, (c,d) 1LP, and (e), (f) 4LP specimens. (Images b, d and f illustrate the pile-up formation around the residual impressions)—For a better demonstration, samples were titled at 40°. In this view, it may seem that pile-ups have non-uniformly been generated on just one side, but it should be noted that the pile-up has occurred adjacent to the other edges as well.

can be seen in table3. It was observed that 4LP has a higher level of surface compressive residual stress (−616 MPa) compared with the 1LP (−540 MPa) and No LP (−203 MPa) specimens. Extreme plastic deformation and high-density dislocations that result from LP can influence high amplitude compressive stresses [31]. These compressive residual stresses might act as a shield against the penetration of the nanoindenter tip [30]. Hence, the No LP specimen, which has comparatively less compressive residual stresses, is more likely to undergo a higher level of plastic deformation than the LPed specimens during the cyclic indentation.

As shown in figure 4, in the early cycles, the reload curves present a lower displacement than the unloading curves. This forms a hysteresis loop between the unloading and reloading curves of cycles. For all specimens, it was found that the area of the hysteresis loop increased slightly during the first several cycles and then began to significantly drop. Hysteresis during multicycle nanoindentation of different materials can originate from fracture and the formation of surface cracks [22], phase transformation [32, 33], and reverse plasticity (plastic deformation that occurs during unloading) [34–36]. However, it is unlikely that Inconel superalloys will undergo any phase transformation under stress at room temperature [23]. No fracture or surface cracking was detected around the indents for all three specimens (figure 5). Hence, it seems that the origin of distinct hysteresis behavior is direct evidence of non-purely elastic behavior in the material during the unloading.

Figures 5(a)–(c) show the pile-up formation around the indent in the No LP, 1LP, and 4LP specimens, respectively. The uniformity in the pile-up

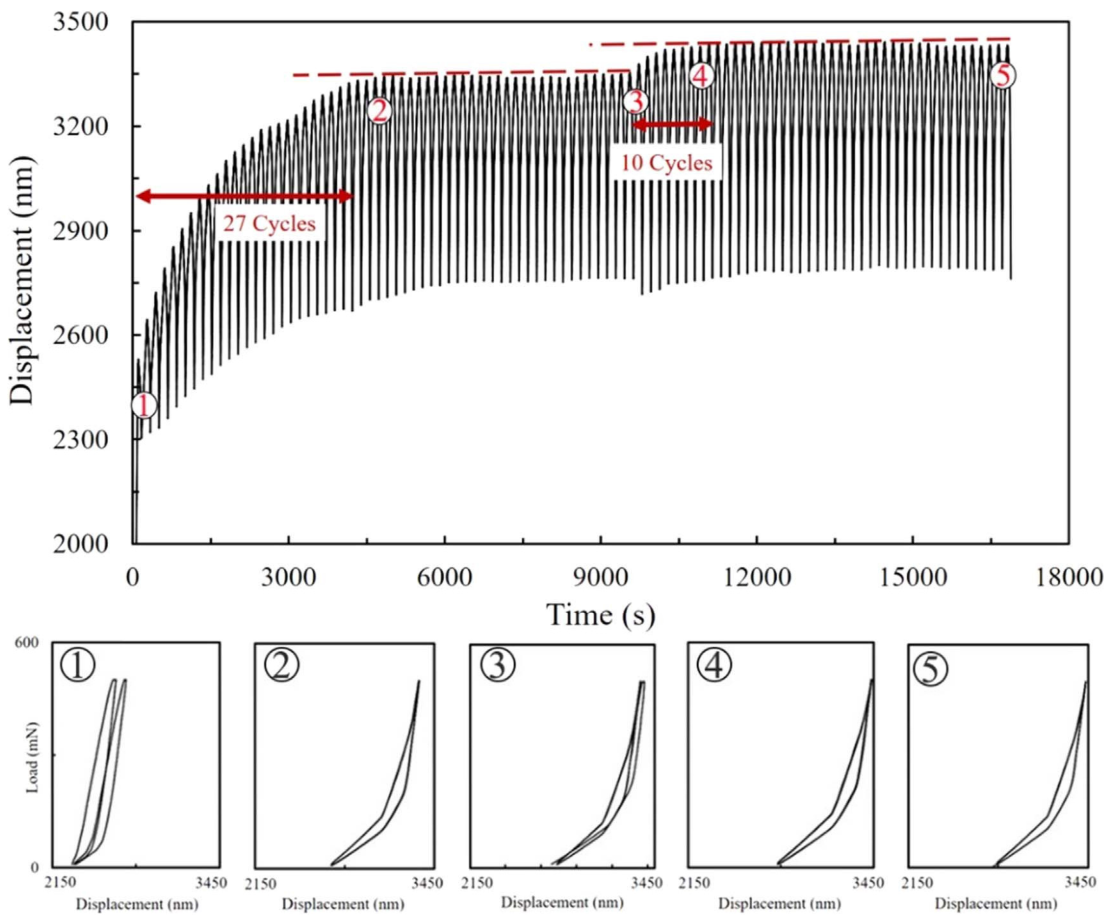

Figure 6. Depth versus time curves of No LP specimen (The load-displacement graph for each points represents two cycles).

surrounding the 4LP indent, cannot be observed in the No LP and 1LP specimens. In previous research by Hu *et al* it was reported that grain size can affect the pile-up formation during indentation [37]. During the laser peening process, grain modifications occur at the surface and just beneath the surface of the material. In addition, the laser peening process and the induced dislocations encourage the formation of the sub-grains [38]. Repeated pressure waves, due to multiple cycles of laser peening, lead to the formation of numerous shear bands, which act to promote the division of sub-grains into fine grains achieving further refinement of the surface grains [16, 17]. It is hypothesized that finer grains, in addition to the presence of sub-grains in the 4LP specimen, may lead to a more pronounced pile-up in comparison to the pile-up that is presented in the 1LP and No LP specimens. However, this phenomenon is still not well understood and requires further investigation using techniques such as *in situ* SEM and transmission electron microscopy (TEM).

Figures 6–8 show typical depth versus time curves of the No LP and LPed specimens during the multi-cycle tests. Generally, the indentation depth-time curves can be divided into the early transient stage and the subsequent steady-state stage [24]. It is observed that during the early transient stage, the indentation penetration depth nonlinearly increased with time for all the No LP and LPed specimens, which implies plastic deformation occurred in this stage, and then the variation of penetration depth became negligible in the steady stage, which implies the plastic deformation was stabilized in the steady stage.

For the No LP specimen (figure 6), the indentation penetration depth increased subsequently in the first 27 cycles to a maximum penetration of 3350 nm. According to load-displacement curves, the material has an elastic-plastic behavior during these cycles (Point 1 to 2). Then, during the next 30 cycles (Point 2 to 3), the maximum depth was almost constant (steady-stage), meaning that the loops appear to overlap. In these cycles, the material behavior converts to almost entirely elastic so that after reaching the maximum depth, the tip returns to its original position during the unloading (figure 6 (load-displacement curves at point 2)). In fact, the area enclosed in these loops represents the irreversible consumption of energy required to open and close the non-propagating crack under the indenter tip during loading/unloading. Again, the maximum depth increased nonlinearly in the next 10 cycles (Point 3 to 4) until reaching a constant maximum penetration of 3420 nm during the rest of the cycles (Point 4 to 5). This sudden plastic deformation between cycles 57 and 67 in the

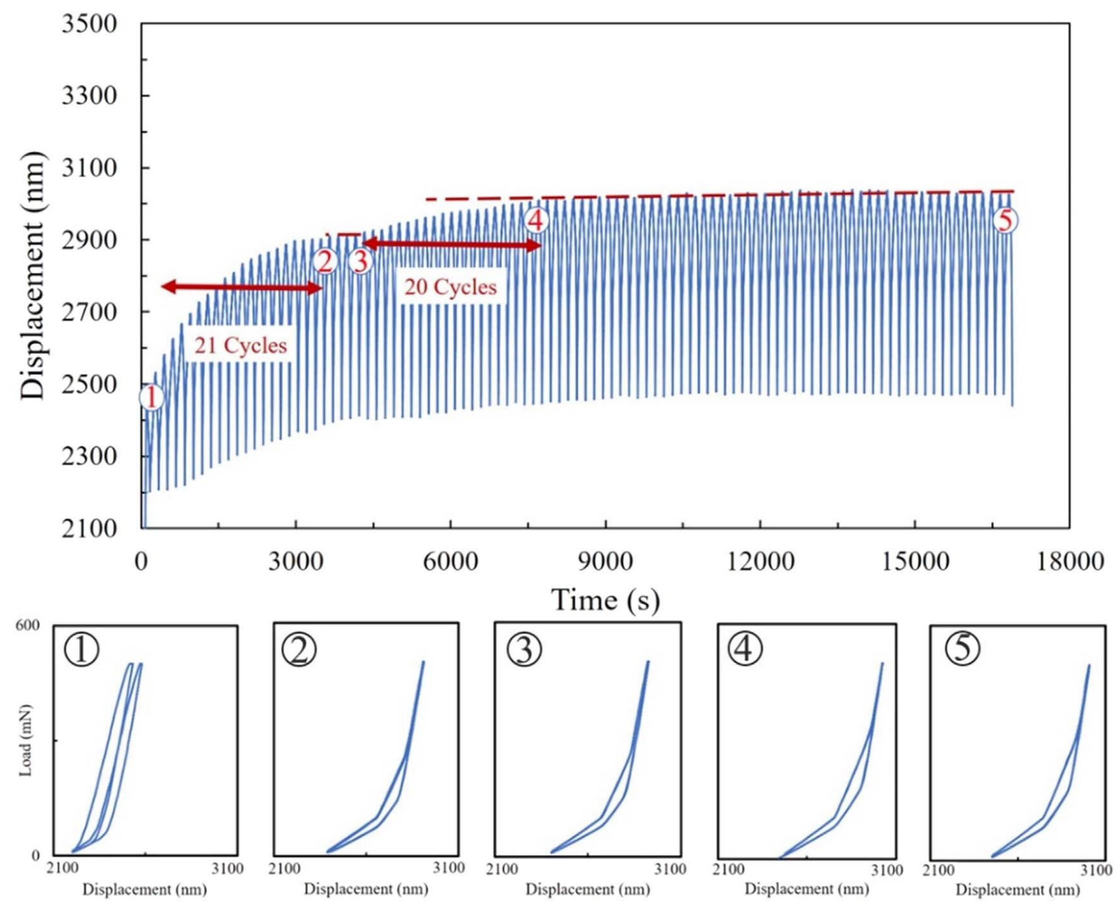

Figure 7. Depth versus time curves of 1LP specimen (The load –displacement graph for each points represents two cycles).

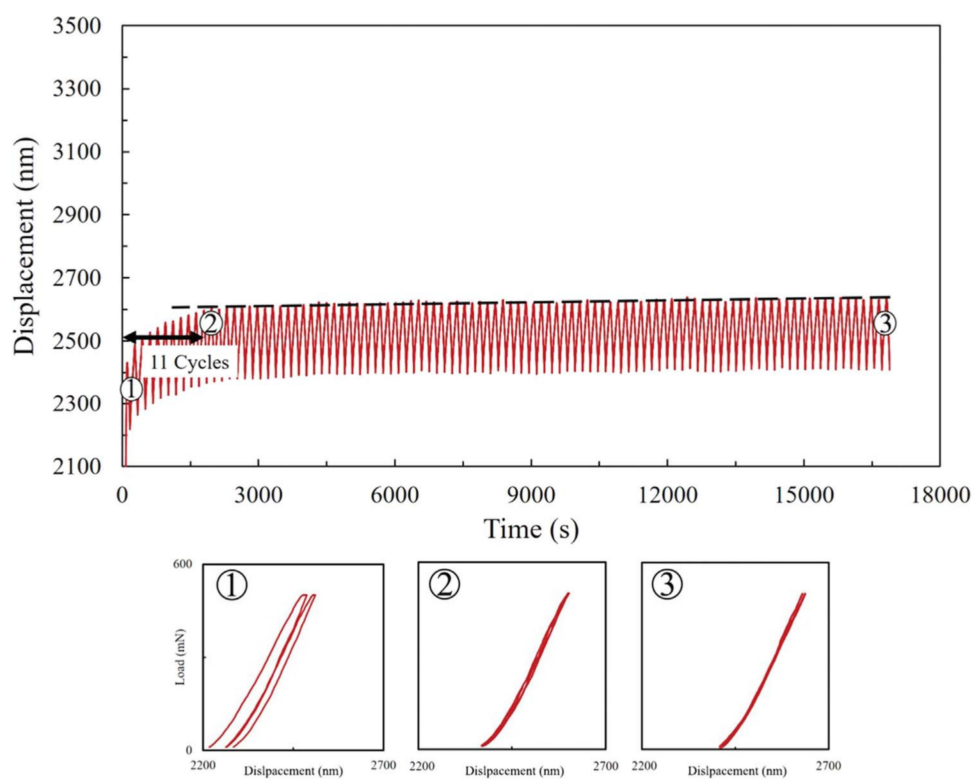

Figure 8. Depth versus time curves of 4LP specimen (The load-displacement graph for each points represents two cycles).

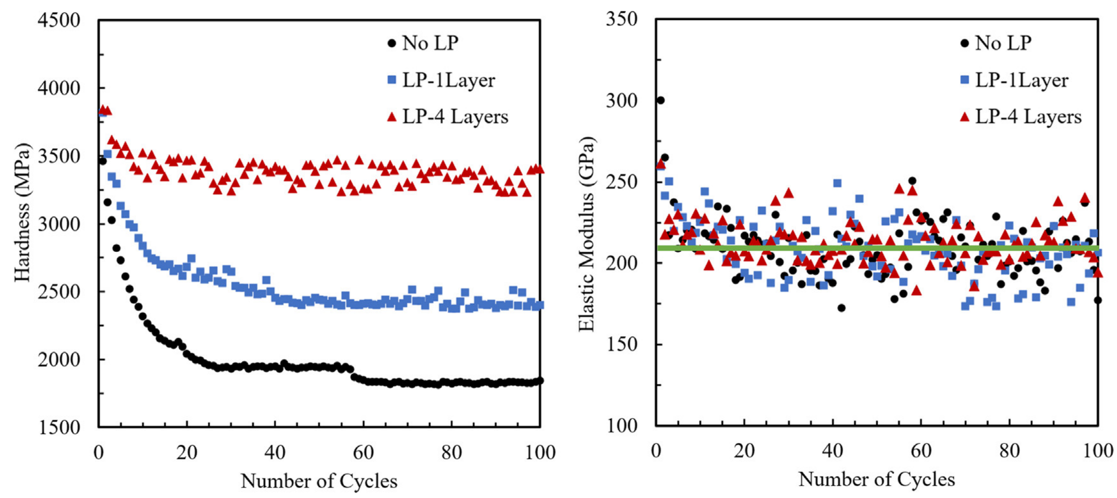

Figure 9. Variation of (a) Nanohardness and (b) Elastic modulus during multicycle indentation.

No LP specimen might be due to the small amount of crack propagation and local yielding of the material under the indenter tip. During the rest of the cycles, again the material behaves almost entirely elastic.

During the first 21 cycles (Point 1 to 2) of the multicycle test for the 1LP specimen (figure 7), the indentation penetration depth increased nonlinearly until reaching a constant depth which remained constant for 4 cycles (Point 2 to 3). After this, a nonlinear increase in depth occurred once again for 20 cycles (Point 3 to 4) until reaching a constant maximum penetration of 3000 nm during the remaining cycles (Point 4 to 5). Similar to the No LP specimen, the material behavior in the early stage of cycles is elastic-plastic. After reaching the steady stage, the material behaved almost entirely elastic in each cycle, and only a small amount of plastic deformation was observed.

For the 4LP specimen in figure 8, the indentation penetration depth only increased during the first 11 cycles of indentation (Point 1 to 2) until reaching a maximum penetration depth of 2600 nm. Upon reaching a depth of 2600 nm, the depth remained almost constant during the remaining cycles (Point 2 to 3). The maximum plastic deformation in the 4LP specimen was experienced during the first 12 cycles of indentation, followed by negligible plastic deformation in the remaining cycles. The material behavior converted from elastic-plastic to almost purely elastic where the displacement is almost completely recovered during unloading. In fact, it can be observed that in the remainder of the steady stage cycles, plasticity or fracture in the material is seemingly negligible due to the almost entirely elastic deformation that occurred.

A higher immobile dislocation density in the 4LP specimen compared to the 1LP and No LP specimens resulted in a faster and stronger interaction of dislocations which work-hardened the material quicker, leading to a larger resistance to the penetration of the indenter and propagation of the plastic zone [24]. Moreover, the higher level of compressive residual stress in LPed specimens increased the force required for plastic deformation during the indentation. Therefore, by increasing the resistance of the material against deformation, the permanent penetration depth of the indenter was decreased.

Figure 9(a) shows the variation of nanohardness during the multicycle test. The values of nanohardness tend to decrease as the number of cycles increases until finally reaching a constant value for all three specimens. It can be observed that the LPed specimens have higher hardness compared to the No LP specimen. Assuming that the dislocations will obstruct the dislocation motion, this behavior can be attributed to the higher density of dislocations created during LP that work hardens the material and increases the local hardness. A higher level of dislocation density after 4-layer laser peening leads to higher hardness in comparison to single-layer laser peening.

Figure 9(b) shows the elastic modulus for nanoindentation obtained from multicycle tests for all specimens. It was observed that the elastic modulus did not change significantly due to laser peening. The green line in the graph displayed in figure 9(b) is the tensile test elastic modulus which was obtained from reference literature [39, 40]. The average values of elastic modulus were 209.72 GPa, 209.04 GPa, and 213.40 GPa for No LP, 1LP, and 4 LP respectively, which is approximately equal the tensile test elastic modulus of 206 MPa.

4. Conclusions

- It has been determined that multicycle tests are very valuable for investigating material behavior by providing additional insight to what can be observed from single-cycle load-displacement curves which cannot be easily identified using microscopy.

- LP can effectively prevent plastic deformation during the multicycle test, and the surface fatigue resistance increases with increasing number of impacts.
- Improved material behavior in LPed specimens can be attributed to the combined effects of the compressive residual stresses and work hardening that were induced during the LP process which produce higher resistance to penetration of the indenter and permanent deformation during cyclic indentation.
- The plastic deformation during the indentation generally saturated after several cycles and then transitioned to almost entirely elastic. This occurred at lower cycles in the 4LP specimen as compared to the No LP and 1LP specimen.
- The Hardness values were found to increase for the LPed specimens while the elastic modulus was found to not change significantly with LP.

Acknowledgments

The authors would like to acknowledge the Alabama Transportation Institute for the continual support of the researchers responsible for authoring this work. The project has also received additional support from the National Science Foundation, CMMI, Advanced Manufacturing Program (Award number: 2029059).

Data availability statement

The data that support the findings of this study are available upon reasonable request from the authors.

ORCID iDs

Kasra Momeni https://orcid.org/0000-0002-4209-1129
Keivan Davami https://orcid.org/0000-0003-2123-8192

References

[1] Li S, Wei Q, Shi Y, Chua C K, Zhu Z and Zhang D 2015 Microstructure characteristics of inconel 625 superalloy manufactured by selective laser melting *J. Mater. Sci. Technol.* **31** 946–52

[2] Shankar V, Bhanu Sankara Rao K and Mannan S L 2001 Microstructure and mechanical properties of Inconel 625 superalloy *J. Nucl. Mater.* **288** 222–32

[3] Rowe R A, Tajyar A, Munther M, Johanns K E, Allison P G, Momeni K and Davami K 2021 Nanoscale serration characteristics of additively manufactured superalloys *J. Alloys Compd.* **854** 156723

[4] Song K H and Nakata K 2010 Effect of precipitation on post-heat-treated Inconel 625 alloy after friction stir welding *Mater. Des.* **31** 2942–7

[5] Dinda G P, Dasgupta A K and Mazumder J 2009 Laser aided direct metal deposition of Inconel 625 superalloy: microstructural evolution and thermal stability *mater. sci. eng. a* **509** 98–104

[6] Gonzalez J A, Mireles J, Stafford S W, Perez M A, Terrazas C A and Wicker R B 2019 Characterization of Inconel 625 fabricated using powder-bed-based additive manufacturing technologies *J. Mater. Process. Technol.* **264** 200–10

[7] Mumtaz K A and Hopkinson N 2010 Selective Laser Melting of thin wall parts using pulse shaping *J. Mater. Process. Technol.* **210** 279–87

[8] Yadroitsev I, Thivillon L, Bertrand P and Smurov I 2007 Strategy of manufacturing components with designed internal structure by selective laser melting of metallic powder *Appl. Surf. Sci.* **254** 980–3

[9] Tian Z, Zhang C, Wang D, Liu W, Fang X, Wellmann D, Zhao Y and Tian Y 2020 A review on laser powder bed fusion of inconel 625 nickel-based alloy *Appl. Sci.* **10** 81

[10] Xing X, Duan X, Jiang T, Wang J and Jiang F 2019 Ultrasonic peening treatment used to improve stress corrosion resistance of AlSi10Mg components fabricated using selective laser melting *Metals (Basel)* **9** 103

[11] Chen T, John H, Xu J, Lu Q, Hawk J and Liu X 2013 Influence of surface modifications on pitting corrosion behavior of nickel-base alloy 718. Part 1: Effect of machine hammer peening *Corros. Sci.* **77** 230–45

[12] Kumagai M, Curd M E, Soyama H, Ungár T, Ribárik G and Withers P J 2021 Depth-profiling of residual stress and microstructure for austenitic stainless steel surface treated by cavitation, shot and laser peening *Mater. Sci. Eng. A* **813** 141037

[13] Gao Y K 2011 Improvement of fatigue property in 7050-T7451 aluminum alloy by laser peening and shot peening *Mater. Sci. Eng. A* **528** 3823–8

[14] Liu K K and Hill M R 2009 The effects of laser peening and shot peening on fretting fatigue in Ti-6Al-4V coupons *Tribol. Int.* **42** 1250–62

[15] Hu Y, Cheng H, Yu J and Yao Z 2020 An experimental study on crack closure induced by laser peening in pre-cracked aluminum alloy 2024-T351 and fatigue life extension *Int. J. Fatigue* **130** 105232

[16] Sheng J, Zhang H, Hu X and Huang S 2020 Influence of laser peening on the high-temperature fatigue life and fracture of Inconel 718 nickel-based alloy *Theor. Appl. Fract. Mech.* **109** 102757

[17] Trdan U, Skarba M and Grum J 2014 Laser shock peening effect on the dislocation transitions and grain refinement of Al-Mg-Si alloy *Mater. Charact.* **97** 57–68

[18] Munther M, Martin T, Tajyar A, Hackel L, Beheshti A and Davami K 2020 Laser shock peening and its effects on microstructure and properties of additively manufactured metal alloys: A review *Eng. Res. Express.* **2** 022001

[19] Faisal N H, Prathuru A K, Goel S, Ahmed R, Droubi M G, Beake B D and Fu Y Q 2017 Cyclic nanoindentation and nano-impact fatigue mechanisms of functionally graded TiN/TiNi film *Shape Mem. Superelasticity.* **3** 149–67

[20] Khlifi K, Barhoumi N, Dhiflaoui H and Ben Cheikh Larbi A 2021 Fatigue behaviour and mechanical properties of PVD CrSiN coating using cyclic nanoindentation *Tribol. - Mater. Surfaces Interfaces* **15** 252–7

[21] Jose F, Ramaseshan R, Balamurugan A K, Dash S, Tyagi A K and Raj B 2011 Continuous multi cycle nanoindentation studies on compositionally graded Ti1-xAlxN multilayer thin films *Mater. Sci. Eng. A* **528** 6438–44

[22] Richter A, Daghlian C P, Ries R and Solozhenko V L 2006 Investigation of novel superhard materials by multi-cycling nanoindentation *Diam. Relat. Mater.* **15** 2019–23

[23] Chatterjee A, Srivastava M, Sharma G and Chakravartty J K 2014 Investigations on plastic flow and creep behaviour in nano and ultrafine grain Ni by nanoindentation *Mater. Lett.* **130** 29–31

[24] Peng L 2005 *Indentation and impression fatigue of aluminum processed by equal channel angular extrusion* University of Kentucky (https://search.proquest.com/openview/

6117749e74cdc7cf9cf2951c7034e532/1?pq-origsite=gscholar&cbl=18750&diss=y)

[25] Sundar R, Kumar H, Kaul R, Ranganathan K, Tiwari P, Kukreja L M and Oak S M 2012 Studies on laser peening using different sacrificial coatings *Surf. Eng.* **28** 564–8

[26] Prabhakaran S and Kalainathan S 2016 Compound technology of manufacturing and multiple laser peening on microstructure and fatigue life of dual-phase spring steel *Mater. Sci. Eng. A* **674** 634–45

[27] Zhang X C, Zhang Y K, Lu J Z, Xuan F Z, Wang Z D and Tu S T 2010 Improvement of fatigue life of Ti-6Al-4V alloy by laser shock peening *Mater. Sci. Eng. A* **527** 3411–5

[28] Kramer D, Huang H, Kriese M, Robach J, Nelson J, Wright A, Bahr D and Gerberich W W 1998 Yield strength predictions from the plastic zone around nanocontacts *Acta Mater.* **47** 333–43

[29] Zielinski W, Huang H and Gerberich W W 1993 Microscopy and microindentation mechanics of single crystal Fe-3 wt% Si: Part II. TEM of the indentation plastic zone *J. Mater. Res.* **8** 1300–10

[30] Zhou J Z, Huang S, Sheng J, Lu J Z, Wang C D, Chen K M, Ruan H Y and Chen H S 2012 Effect of repeated impacts on mechanical properties and fatigue fracture morphologies of 6061-T6 aluminum subject to laser peening *Mater. Sci. Eng. A* **539** 360–8

[31] Zhou J Z, Huang S, Zuo L D, Meng X K, Sheng J, Tian Q, Han Y H and Zhu W L 2014 Effects of laser peening on residual stresses and fatigue crack growth properties of Ti–6Al–4V titanium alloy *Opt. Lasers Eng.* **52** 189–94

[32] Arciniegas M, Gaillard Y, Peña J, Manero J M and Gil F J 2009 Thermoelastic phase transformation in TiNi alloys under cyclic instrumented indentation *Intermetallics* **17** 784–91

[33] Gogotsi Y G, Domnich V, Dub S N, Kailer A and Nickel K G 2000 Cyclic nanoindentation and Raman microspectroscopy study of phase transformations in semiconductors *J. Mater. Res.* **15** 871–9

[34] Huang Y, Tjahyono N I, Shen J and Chiu Y L 2008 Reverse plasticity in nanoindentation in*Mater. Res. Soc. Symp. Proc., Cambridge University Press* 135–40

[35] Shuman D J, Costa A L M and Andrade M S 2007 Calculating the elastic modulus from nanoindentation and microindentation reload curves *Mater. Charact.* **58** 380–9

[36] Oliver W C and Pharr G M 1992 An improved technique for determining hardness and elastic modulus using load and displacement sensing indentation experiments *J. Mater. Res.* **7** 1564–83

[37] Hu J, Zhang Y, Sun W and Zhang T 2018 Nanoindentation-induced pile-up in the residual impression of crystalline Cu with different grain size *Crystals.* **8** 9

[38] Munther M, Russell A R, Sharma M, Hackel L and Davami K 2020 Thermal stabilization of additively manufactured superalloys through defect engineering and precipitate interactions *Mater. Sci. Eng. A* **798** 140119

[39] Data sheet: In625-0402 powder for additive manufacturing: AMPD AM 3d printing metal powder AM250, (n.d) (https://resources.renishaw.com/enfdetails/data-sheet-in625-0402-powder-for-additive-manufacturing–97039) (accessed July 1, 2021)

[40] Neu R W, Antoniou A and Stebner A 2020 *High Cycle Fatigue of Additively Manufactured Inconel, Georgia Institute of Technology* **625** (https://smartech.gatech.edu/handle/1853/64193) (accessed July 1, 2021)